Polyaromatic cores for the exfoliation of popular 2D materials†

Marina Garrido, *[a] Myriam Barrejón, [a,b] José Augusto Berrocal, [c] Zois Syrgiannis[a,d,e] and Maurizio Prato [a,f,g]

Two-dimensional (2D) nanomaterials have attracted interest from the scientific community due to their unique properties. The production of these materials has been carried out by diverse methodologies, the liquid phase exfoliation being the most promising one due to its simplicity and potential scalability. The use of several stabilizers allows to obtain dispersions of these 2D nanomaterials in solvents with low boiling points. Herein we describe a general exfoliation method for different 2D materials employing a biphasic water/dichloromethane system and two different (poly)aromatic hydrocarbons (PAHs). This method allows us to obtain dispersions of the exfoliated 2D materials with high concentrations in the organic solvent. Due to the low boiling point of dichloromethane, and therefore its easy removal, the obtained dispersions can be employed as additives for different composites. We corroborate that the exfoliation efficiency is improved due to the π–π and van der Waals interactions between the PAHs and the layers of the 2D materials.

Introduction

Since the isolation of graphene by mechanical exfoliation of graphite in 2004,[1] other layered materials such as graphitic carbon nitride (g-C_3N_4),[2] boron nitride (BN)[3] or transition metal dichalcogenides (MoS_2)[4,5] have attracted attention from the scientific community. All these materials present specific characteristics, their lamellar structure being one of the most important characteristics, similar to that of graphite. Their morphology allows their exfoliation into two-dimensional (2D) nanomaterials with intriguing properties. For example, BN is an insulating material with a large band gap (5–6 eV)[6] and presents a high thermal conductivity (2000 W m^{-1} K^{-1}),[7] being suitable as a dielectric substrate in electronic devices,[8] as a filler to enhance the thermal conductivity of composites[9] or as a catalyst in different reactions.[10,11] A single layer of MoS_2 has a direct semiconductor band gap of 1.8 eV and a strong photoluminescence.[12] Due to their electronic and optical properties, MoS_2 flakes have been applied in field effect transistors,[13,14] electrocatalysis[15,16] and optoelectronic devices,[17,18] among others. In the case of g-C_3N_4, the exfoliated nanosheets also exhibit enhanced properties with respect to the bulk. The delaminated material possesses high photoluminescence quantum yields and shows an increment in the value of its band gap (around 2.7–2.8 eV, depending on the synthetic procedures).[19,20] These interesting properties, along with the largest surface area of the nanosheets, allow the application of g-C_3N_4 in bioimaging and different photocatalytic purposes.[19,21–24]

However, most of these 2D materials consist of multilayered structures in their bulk form and all these fascinating features cannot be exploited. For this reason their exfoliation into thin layers is necessary. The generation of these atomically thin 2D nanosheets can be achieved by different methods, which are mainly distinguished in two general categories: bottom-up and top-down approaches. As an example, the weak bonds that hold the multilayers together can be disrupted by mechanical cleavage or liquid phase exfoliation (LPE), two well-known top-down approaches.[25] LPE is an appealing method due to its simplicity, versatility and potential scalability.[26–28] However, the most common solvents employed in the LPE method (NMP, DMF, *etc.*) are expensive and toxic, and have high boiling points and are therefore difficult to remove, hampering

[a]*Department of Chemical and Pharmaceutical Sciences, INSTM UdR Trieste, Università degli Studi di Trieste, Via Licio Giorgieri 1, Trieste 34127, Italy. E-mail: mgarrido@units.it*
[b]*Neural Repair and Biomaterials Laboratory, Hospital Nacional de Parapléjicos (SESCAM), Finca la Peraleda s/n, 45071 Toledo, Spain*
[c]*Adolphe Merkle Institute, University of Fribourg, Chemin des Verdiers 4, 1700 Fribourg, Switzerland*
[d]*Simpson Querrey Institute for BioNanotechnology, Northwestern University, Chicago, IL 60611, USA*
[e]*Department of Chemistry, Northwestern University, Evanston, IL 60208, USA*
[f]*Center for Cooperative Research in Biomaterials (CIC biomaGUNE), Basque Research and Technology Alliance (BRTA), Paseo de Miramón 194, Donostia-San Sebastián 20014, Spain*
[g]*Ikerbasque, Basque Foundation for Science, Bilbao 48013, Spain*
†Electronic supplementary information (ESI) available: Supplementary Fig. S1–S20. See DOI: https://doi.org/10.1039/d2nr00894g

the use of the obtained exfoliated materials in a wide number of applications. For this reason, the search of more suitable solvents is required in order to obtain easily workable dispersions. A promising approach that has not been extensively explored is the use of solvent mixtures, where two solvents with low exfoliation ability are mixed to obtain strong cosolvents that afford stable dispersions of the exfoliated 2D materials.[29] In general, alcohols/water combinations are employed in this strategy, where the alcohol acts as a surfactant, stabilizing the obtained suspension.[30,31] The use of biphasic systems is also a promising alternative.[32] In this case, the two solvents also exhibit low exfoliation ability but are immiscible between them (water/chloroform, water/heptane, and water/dichloromethane). The exfoliation and stabilization of the 2D materials occur by a different pathway in which the two immiscible solvents form an emulsion with a great interfacial area during the sonication process. To minimize the interfacial free energy of the system, the sheets of the 2D material exfoliated during this process are adsorbed at the interface of both solvents, forming stable dispersions.[33] This strategy is known as the solvent interfacial trapping method (SITM) and has been reported to be useful for obtaining films of graphene with controlled thickness,[34] conductive foams[35] and inks.[36]

Other approaches focused on the use of stabilizers,[37] such as surfactants,[38] polymers[39] or organic molecules.[40,41] These compounds avoid the re-aggregation of the 2D materials in common solvents such as water or THF and allow the synthesis of new hybrid materials.[42–44] The interaction between the 2D materials and organic or inorganic molecules takes place through physisorption, chemisorption or electrostatic interactions[45–48] and is accompanied by an adjustment of the properties of both components. In the case of (poly)aromatic hydrocarbons (PAHs), van der Waals and π–π interactions dominate the supramolecular assembly with the 2D materials.[44] Due to their planar structure, PAHs can interact with the layers of the 2D materials and stabilize the resulting dispersions.[49] In fact, it has been demonstrated that the amount of exfoliated material in a dispersion is linearly correlated with the adsorption free energy of the PAHs onto the surface of the 2D materials, meaning that the exfoliation is based on an effective non-covalent binding that maximizes the π–π interactions.[50,51] Furthermore, under the same experimental conditions, the graphene/stabilizer concentration in a dispersion achieved by using PAHs considerably exceeded that of the conventional nanomaterial stabilizers such as surfactants or polymers.[52] Among the different PAHs that have been employed in LPE processes,[41,49,51] naphthalene and perylene diimides (NDI and PDI, respectively) have shown promise for the exfoliation and stabilization of graphite in different solvents. For example, the use of charged NDI derivatives has allowed the isolation of graphene in water or DMF.[53,54] Making use of neutral NDI compounds, graphite can be also exfoliated in $CHCl_3$.[55,56] In the case of PDI, several derivatives have been utilized for the exfoliation of pristine graphite in solvents with different polarities.[57] As an example, with cationic derivatives it is possible to obtain dispersions in water,[58,59] while other types of PDIs allow the simultaneous exfoliation and functionalization of graphene in NMP and *o*-DCB.[60,61] Moreover, with the assistance of PDIs, the exfoliation and stabilization of graphene in common organic solvents ($CHCl_3$, EtOH, *etc.*) is feasible.[62–64] Although widely used for the exfoliation of graphite, the employment of PDI and NDI derivatives for the exfoliation of other 2D materials has been relatively unexplored, and only a few examples have been described in the literature, involving BN,[65] g-C_3N_4 [66] and black phosphorus.[67] Furthermore, to the best of our knowledge, the SITM has only been employed in the exfoliation of graphite, and few examples combine this methodology with the presence of stabilizers.[68,69]

Herein we describe a general exfoliation method for layered 2D materials (graphite, g-C_3N_4, BN and MoS_2) in the presence of two different aromatic cores (**C_{10}-NDI-C_{10}** and **C_{10}-PDI-C_{10}**, Fig. 1). The exfoliation is accomplished in a water/dichloromethane (H_2O/DCM) biphasic system, at room temperature and with short sonication times. Dispersions of 2D materials with high concentrations (up to 1.43 mg mL^{-1}) in a low boiling point solvent have been obtained, thanks to the sum of the effects from the SITM and stabilizers. The resulting hybrid structures have been characterized and the differences between the two aromatic cores have been analyzed. The results confirm that both PAHs interact with the layers of the different 2D materials, promoting their exfoliation and stabilization in DCM through π–π and van der Waals interactions.

Results and discussion

Synthesis and exfoliation method

The synthesis of NDI and PDI derivatives was carried out by the condensation of the desired tetracarboxylic dianhydride with decylamine in order to improve the solubility of the aromatic cores in organic solvents, since they tend to aggregate *via* strong π–π interactions (see the Experimental section for specific details). A reported procedure was applied for **C_{10}-**

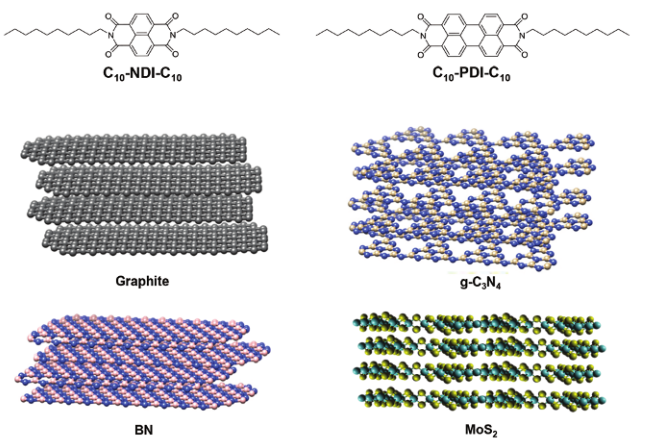

Fig. 1 Structures of the aromatic cores and schematic representation of the bulk materials.

NDI-C_{10},[70] while for **C_{10}-PDI-C_{10}** the synthetic method was a modification of a previous procedure.[71] The exfoliation of four different layered materials (graphite, g-C_3N_4, BN and MoS_2) was performed in a H_2O/DCM (volume ratio 5/2) biphasic system in the presence of the two aromatic cores (**C_{10}-NDI-C_{10}** or **C_{10}-PDI-C_{10}**). In a first step, a dispersion of the bulk material in deionized water was obtained after 30 minutes of sonication. Thereafter, a solution of the corresponding aromatic core in DCM was added, affording two well-separated phases: the aqueous phase where the bulk layered material was suspended, and the organic phase where the aromatic compound was dissolved. In parallel, the same methodology was performed in the absence of the aromatic cores, with the aim of determining their role in the process. This mixture was sonicated for 2 hours, during which the exfoliated layered material moved to the organic phase, while the aqueous phase resulted in having a colorless transparent appearance (ESI Fig. S2†).

It is well known that the exfoliation of 2D materials can be achieved by overcoming the van der Waals interactions between layers, a process that can be performed by LPE in an ultrasonic bath.[72] In the method described here, the exfoliation process can be explained as follows: (1) during the sonication process, an unstable emulsion of DCM in water is produced, with a great number of drops and bubbles that increase the interfacial area of the system. Here, the sheets of the 2D materials are adsorbed at the liquid–liquid interphase of the drops and their restacking is avoided due to the gain in the interfacial energy.[33,73] (2) Due to the hydrophobic nature of the aromatic cores, the π–π and the van der Waals interactions between them and the layered materials are enhanced, minimizing the restacking during and after the sonication. In addition, when the emulsion returns to its stable state (the biphasic system), these non-covalent interactions and the hydrophobicity of the molecules afford dispersions of the 2D materials in DCM with high concentrations (see below).[68,69]

It is worth mentioning that despite the exfoliation mechanism is expected to be similar for the four studied materials, several differences in the interaction with the two different aromatic cores employed here have to be considered, due to the diverse nature of the chemical bonds in the layered materials.[51] Despite the lack of further investigations in this regard, we can hypothesize that, in the case of graphene, the pure covalent bonds between carbon atoms lead to a nonpolar material with a charge density equally distributed along the 2D sheets,[74,75] enhancing the π–π interactions.

On the other hand, the different electronegativity between carbon and nitrogen in g-C_3N_4 and between boron and nitrogen in BN results in polar structures with the charge density concentrated in the N atoms (negatively charged) of the 2D materials.[74,76] In these cases, the interactions between the NDI/PDI derivatives with the flat surface of the materials could not only be due to π–π interactions. As a consequence of the electron-deficient aromatic core of these molecules,[77] additional attractive interactions between them and the negative N atoms of the materials could take place, such as polar/π and induced electrostatic interactions.[75]

Finally, in MoS_2, as a consequence of the three atom layered structure, polar and nonpolar interactions could occur among the aromatic molecules and MoS_2. Theoretical calculations demonstrate that the basal plane of MoS_2 is a nonpolar surface, meanwhile the edges of the material are polar.[78] Taking into account these findings, it could be hypothesized that the interaction between the NDI/PDI derivatives with MoS_2 is a sum of π–π interactions in the basal plane of the material and polar/π and induced electrostatic interactions at the edges.

To prove the efficiency of the exfoliation method different characterization techniques were employed, including transmission electron microscopy (TEM), atomic force microscopy (AFM), and Raman spectroscopy.

Morphology of the exfoliated materials

TEM images provided information about the morphology of the exfoliated 2D-sheets. As observed in Fig. 2 and ESI Fig. S3,† the resulting materials consist of random aggregates with a weak contrast, which suggests their exfoliation into few thin layers. In the case of the 2D materials exfoliated in the absence of the organic aromatic cores (ESI Fig. S4†), these aggregates consist of a higher number of layers (darker contrast), confirming that the non-covalent interactions between the PAHs (**C_{10}-NDI-C_{10}** or **C_{10}-PDI-C_{10}**) and the 2D-sheets minimize the restacking of the layers, affording better exfoliated materials.[79]

The thickness of the exfoliated materials was investigated by AFM. Histograms of the average height distribution are found in ESI Fig. S5–S8† and the results are summarized in Table 1. Taking into account that the typical reported thickness for a monolayer of graphene, g-C_3N_4 and MoS_2 deposited onto SiO_2 has an apparent height of ~1,[80] 0.6[81] and 0.7 nm,[82] respectively, and the presence of the aromatic cores, the AFM images allowed us to determine that all the tested materials are exfoliated and consist of few layers (less than 10). Furthermore, similar exfoliation abilities were observed for both aromatic molecules (NDI and PDI).

Raman spectroscopy

Raman analysis was also performed to corroborate the successful exfoliation of the bulk materials in the presence of both **C_{10}-NDI-C_{10}** and **C_{10}-PDI-C_{10}**, and the improvement of the exfoliation ability of the biphasic system in their presence. Each bulk material shows its characteristic Raman signals. The graphite spectrum shows the D (~1350 cm^{-1}), G (~1580 cm^{-1}) and 2D bands (~2700 cm^{-1}). When graphite is exfoliated into graphene, the shape of the 2D band changes, giving information about the number of layers that compose the exfoliated material.[83] Comparing the Raman spectrum of the material obtained after the exfoliation process in the presence of the aromatic molecules and in their absence (Fig. 3 and ESI Fig. S11†), it can be determined that both, **C_{10}-NDI-C_{10}** and **C_{10}-PDI-C_{10}**, improve the exfoliation ability of the biphasic

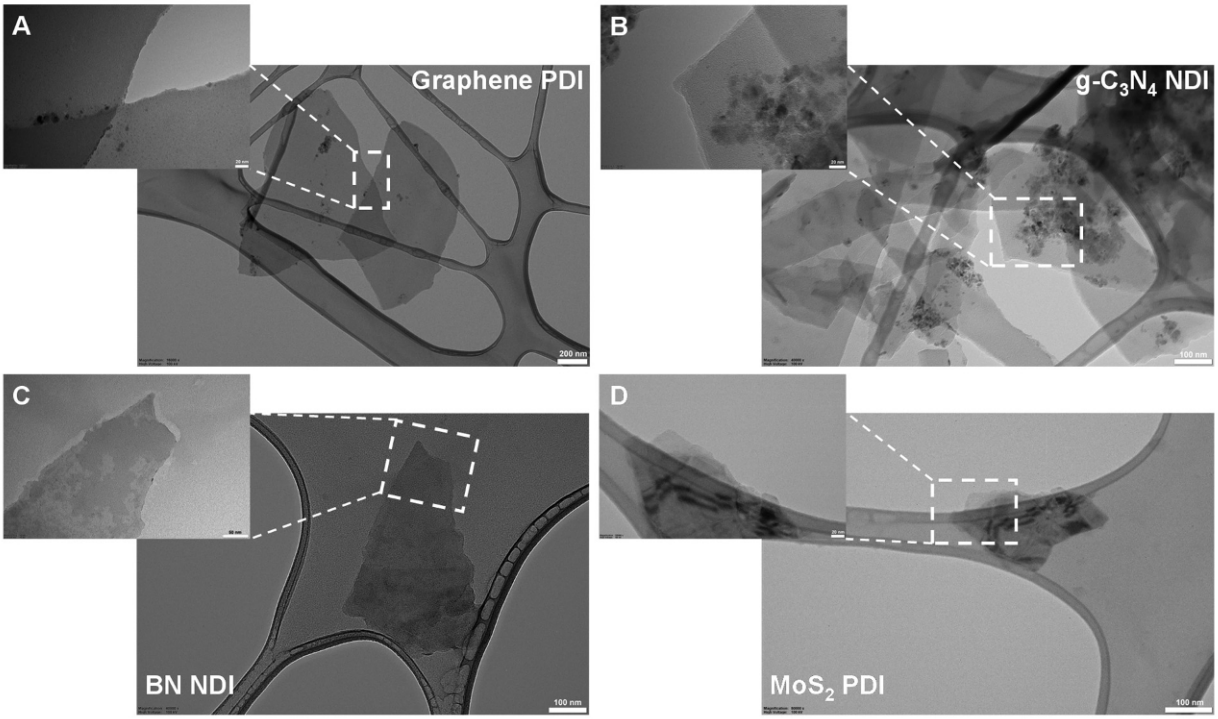

Fig. 2 TEM images of (A) graphene and (D) MoS_2 exfoliated in the presence of **C_{10}-PDI-C_{10}**, (B) g-C_3N_4 and (C) BN exfoliated in the presence of **C_{10}-NDI-C_{10}**. The scale bars are 200 and 20 nm for graphene, 100 and 20 nm for g-C_3N_4, 100 and 50 nm for BN and 100 and 20 nm for MoS_2.

Table 1 Height values obtained with AFM for each 2D material after the exfoliation process

	Height ± SD (nm)
Graphene NDI	8 ± 3
Graphene PDI	10 ± 5
g-C_3N_4 NDI	12 ± 4
g-C_3N_4 PDI	4 ± 2
BN NDI	5 ± 3
BN PDI	5 ± 1
MoS_2 NDI	11 ± 3
MoS_2 PDI	6 ± 2

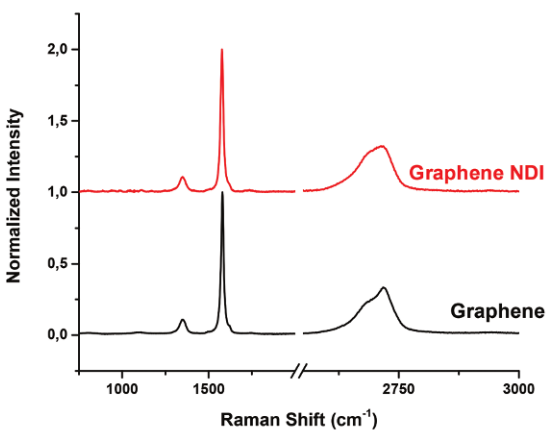

Fig. 3 Average Raman spectra (λ_{exc} = 532 nm) of graphene exfoliated in the presence of **C_{10}-NDI-C_{10}** (red) and in its absence (black).

system. In the case of graphene obtained in the presence of **C_{10}-NDI-C_{10}** (Fig. 3), the average calculated number of layers for the material is 4, while for the material obtained in its absence, the average number of layers is 7.[84] For graphene obtained in the presence of **C_{10}-PDI-C_{10}** (ESI Fig. S11†), the shape change of the 2D band is noticed after the exfoliation, and it can be deconvoluted into four components,[83] confirming the success of the developed method.

The Raman spectrum of g-C_3N_4 is characterized by several peaks located at ~472, 708, 750, 978 and 1233 cm^{-1}. The peaks at 708 and 978 cm^{-1} are attributed to the breathing modes of the s-triazine rings.[85] In order to determine if g-C_3N_4 is exfoliated employing the present methodology, it is necessary to focus on the typical peak located at 707 cm^{-1}. This peak is situated at around 706 cm^{-1} when the exfoliation is performed in the presence of **C_{10}-NDI-C_{10}** or **C_{10}-PDI-C_{10}** (Fig. 4 and ESI Fig. S13†). However, when the exfoliation is carried out in their absence, the former peak is located at around 707 cm^{-1}. The shift to lower frequencies of this peak is due to the phonon confinement effect that occurs when the dimensions of the material decrease,[19] confirming the exfoliation of g-C_3N_4 in the presence of both aromatic molecules.

The characteristic Raman peak of BN is located at ~1365 cm^{-1} (G band, due to its analogy with the G peak of graphene) and corresponds to the E_{2g} vibrational mode of B–N. In spite of the lack of a clear behavior for the Raman results of the exfoliated BN, it was decided to use the results reported by Li and co-workers[86] as a guide, due to the agreement between

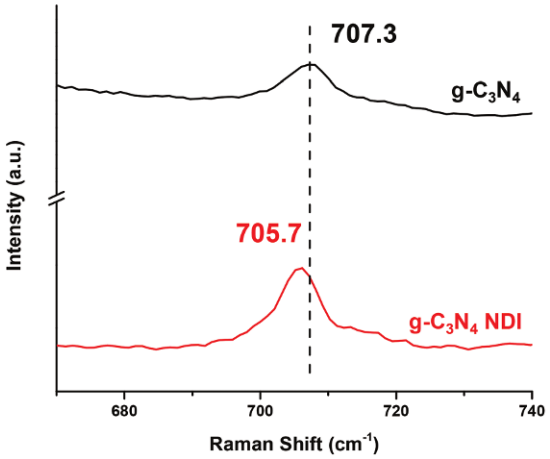

Fig. 4 Average Raman spectra (λ_{exc} = 633 nm) of g-C_3N_4 exfoliated in the presence of **C_{10}-NDI-C_{10}** (red) and in its absence (black).

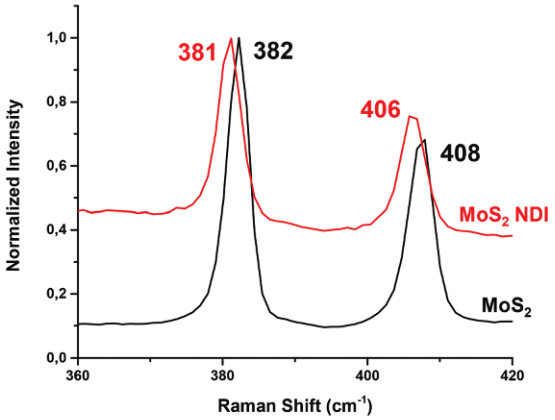

Fig. 6 Average Raman spectra (λ_{exc} = 785 nm) of MoS_2 exfoliated in the presence of **C_{10}-NDI-C_{10}** (red) and in its absence (black).

the experimental results and the theoretical calculations. When the number of layers decreases, meaning when the material is exfoliated, the G band of BN shifts to higher frequencies and the full width at half maximum (FWHM) increases.[86–88] Comparing the Raman spectrum of BN exfoliated in the presence of **C_{10}-NDI-C_{10}** and in its absence (Fig. 5), one can observe the shift to higher frequencies of the G band, and an increase of the FWHM from 10.70 (BN exfoliated in the absence of the molecule) to 12.34 (BN exfoliated in the presence of **C_{10}-NDI-C_{10}**). In the case of the exfoliation in the presence of **C_{10}-PDI-C_{10}** (ESI Fig. S15†), the G band is also shifted to higher frequencies and the FWHM increases from 12.35 (BN exfoliated in the absence of the molecule) to 13.52 (BN exfoliated in the presence of **C_{10}-PDI-C_{10}**). These results confirm the better exfoliation of BN in the presence of both aromatic cores.

In the case of MoS_2, the Raman spectrum is characterized by two peaks located at ~382 cm^{-1} and ~407 cm^{-1}, that correspond to the in-plane (E^1_{2g}) and out-of-plane (A_{1g}) vibration modes, respectively.[39,89,90] As it can be observed in Fig. 6, the spectrum of the exfoliated material in the presence of **C_{10}-NDI-C_{10}** is shifted to lower frequencies when compared with the spectrum of MoS_2 exfoliated in its absence. The same tendency has also taken place after the procedure with **C_{10}-PDI-C_{10}** (ESI Fig. S17†). The shift of both characteristic peaks corroborates the exfoliation of MoS_2 by both aromatic molecules and their possible adsorption on the surface of the 2D material.

Taking into account the results of Raman analyses, it can be concluded that the exfoliation ability of the water/dichloromethane biphasic system improves in the presence of **C_{10}-NDI-C_{10}** and **C_{10}-PDI-C_{10}**.

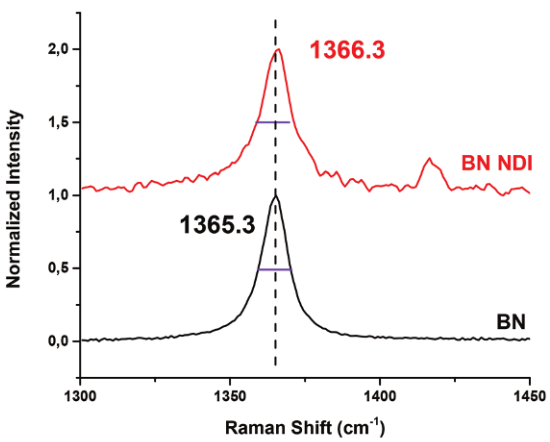

Fig. 5 Average Raman spectra (λ_{exc} = 633 nm) of BN exfoliated in the presence of **C_{10}-NDI-C_{10}** (red) and in its absence (black). In purple is marked the FWHM.

Exfoliation efficiency

In order to determine the exfoliation efficiency for each material, the concentration of the 2D materials in the organic phase (DCM) was determined by gravimetric analysis (see the Experimental section for details). Herein, the amount of the dispersed material in DCM divided by the initial amount of bulk material is defined as an exfoliation yield. As it can be seen in Table 2, both molecules are able to exfoliate the 2D materials in good yields, affording dispersions with higher concentrations than those reported for other volatile solvents.[49,56,64] In general, the concentration of the exfoliated 2D material is higher when **C_{10}-PDI-C_{10}** is employed. This result is in agreement with the linear correlation that exists between the adsorption energy of PAH–graphene and the amount of exfoliated material in a dispersion.[50] Since the aromatic core of the perylene derivative is larger than that of the naphthalene one, its adsorption energy is expected to be greater also,[91] and therefore the concentration of the different 2D materials in the resulting dispersions.

Finally, to prove the interaction between both PAHs and the 2D materials, UV-Vis absorption spectroscopy was performed. Since the exfoliation of the 2D materials was accomplished with an excess of the organic molecules, the hybrid materials

Table 2 Concentrations and yields of the obtained dispersions for each 2D material

	Concentration ± SD (mg mL^{-1}) and (yield (%))			
Aromatic core	Graphene	g-C_3N_4	BN	MoS_2
Without	0.59 ± 0.04 (24)	—	0.15 ± 0.14 (6)	0.35 ± 0.16 (14)
C_{10}-NDI-C_{10}	0.74 ± 0.04 (30)	0.81 ± 0.01 (29)	0.46 ± 0.14 (18)	1.17 ± 0.06 (47)
C_{10}-PDI-C_{10}	0.90 ± 0.02 (36)	0.65 ± 0.06 (26)	0.62 ± 0.03 (25)	1.43 ± 0.03 (57)

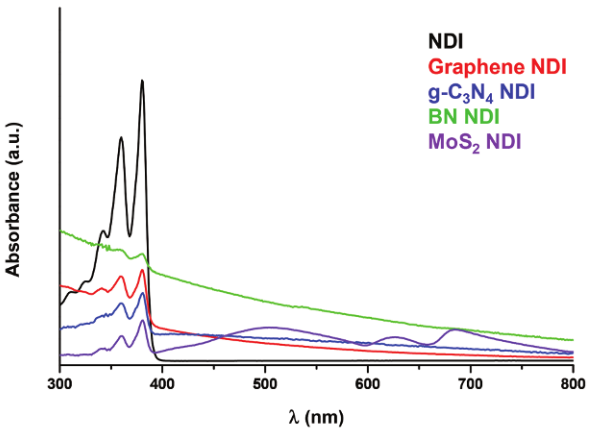

Fig. 7 UV-Vis spectra in DCM of **C_{10}-NDI-C_{10}** (black), graphene NDI (red), g-C_3N_4 NDI (blue), BN NDI (green) and MoS_2 NDI (purple).

were obtained after a washing step to remove the free molecules that were in solution (see the Experimental section). UV-Vis spectra were recorded to determine the presence of the aromatic compounds in the hybrid materials. In the obtained spectra, the absorption bands of **C_{10}-NDI-C_{10}** at 360 and 380 nm, together with the characteristic profile of the corresponding material, were clearly observed (Fig. 7). A similar trend was also present in the case of **C_{10}-PDI-C_{10}** hybrid materials (ESI Fig. S18†), with the absorption bands being located at 488 and 525 nm. These results confirm the interaction between the organic compounds and the 2D materials through π–π and van der Waals interactions.[58]

Conclusions

In summary, the employment of the SITM for the exfoliation of bulk graphite, g-C_3N_4, BN and MoS_2 into few-layered nanosheets has been carried out successfully in the presence of two different aromatic cores (**C_{10}-NDI-C_{10}** and **C_{10}-PDI-C_{10}**) employing a water/dichloromethane biphasic system. The formation of an emulsion during the sonication step allows the exfoliation of the 2D materials using two immiscible solvents in which these materials are hardly dispersed. In addition, the presence of the aromatic cores allows to obtain the dispersions of the 2D materials and avoids re-aggregation in the organic solvent. The characterization was carried out by TEM, AFM and Raman spectroscopy, confirming the successful exfoliation in a volatile solvent like dichloromethane. Further work has to be carried out to determine if any kind of electronic communication exists between the PAHs and the different 2D materials, allowing the future application of the supramolecular hybrids in the field of photovoltaics. Due to the simplicity of the method, the easy isolation of the exfoliated materials, their high concentrations and the facile removal of the solvent, the obtained dispersions can be employed as additives for different composites.

Experimental section

Materials

Graphite flakes used for obtaining expanded graphite and graphene was purchased from SIGMA-ALDRICH (particle size = +100 mesh). Graphite (1 g) was dispersed in *N*-methylpyrrolidone (NMP) (10 mL) and sonicated for 4 hours with a sonic tip (20% amplitude, pulses 30″on–30″off) using an ice bath to avoid the increase of temperature of the dispersion. In order to obtain expanded graphite, this dispersion was filtered under vacuum using nylon (HNWP) (pore size = 0.45 μm, Φ = 47 mm) membranes and subsequently was washed with isopropanol three times. Graphitic carbon nitride (g-C_3N_4) was synthesized following a reported procedure.[20] Boron nitride (BN, particle size ~1 μm) and molybdenum disulfide (MoS_2, particle size <2 μm) were purchased from SIGMA-ALDRICH.

Experimental procedure

General procedure for the exfoliation of different 2D materials. 5 mg of the bulk material (expanded graphite, g-C_3N_4, BN or MoS_2) were dispersed in 5 mL of deionized water and sonicated for 30 minutes in a low-power sonication bath. Subsequently, a solution of 5 mg of **C_{10}-NDI-C_{10}** or **C_{10}-PDI-C_{10}** in 2 mL of dichloromethane (DCM) was added onto the material dispersion and sonicated for 2 hours. After this time, two well defined phases were obtained, the organic phase where all the material was located and the colorless aqueous phase. The characterization of the exfoliated materials was carried out taking a drop of the organic phase and diluting into an additional 2 mL of DCM.

Calculation of the concentrations of the 2D materials in the organic phase. The two phases were extracted in order to separate them. Then, the solvent was removed to know the total mass in each phase. With the aim to know the mass of the 2D materials in the organic phase (DCM), the mass of the organic

molecule (total molecule – molecule in aqueous phase) was subtracted from the total mass in the DCM phase.

Synthesis of the hybrid materials. After the extraction, the organic phase was filtered on a polytetrafluoroethylene (PTFE, pore size = 0.45 μm, Φ = 25 mm) membrane, and washed with DCM until the filtrate was transparent to afford the corresponding hybrid material.

C_{10}-NDI-C_{10} was synthesized using a literature procedure.[70] Synthesis of **C_{10}-PDI-C_{10}:** perylene-3,4,9,10-tetracarboxylic dianhydride (1 g, 2.55 mmol), decylamine (2 mL, 10.2 mmol) and imidazole (5 g) were stirred at 160 °C for 24 hours under Ar atmosphere. The reaction mixture was cooled to room temperature and filtered, and then was washed with hot ethanol and HCl 1 M. Subsequently, the solid obtained was transferred to a flask and a 20% aqueous solution of KOH was added, the mixture was stirred at room temperature for 1 hour and then filtered. Finally, the solid was washed with ethanol affording the desired product with a yield of 96%. ^{1}H-NMR (400 MHz, $CDCl_3$), δ: 8.71 (d, 4H, J = 8.1 Hz), 8.65 (d, 4H, J = 8.1 Hz), 4.23–4.18 (m, 4H), 1.81–1.71 (m, 4H), 1.48–1.22 (m, 28H), 0.87 (t, 6H, J = 6.9 Hz).

All reagents were purchased from commercial sources and used without further purification unless otherwise stated.

Characterization techniques

^{1}H-NMR spectra were recorded at 400 MHz (Varian 400 spectrometer).

Raman spectra were recorded on a Renishaw inVia Raman Microscope at room temperature using an exciting laser source of 532, 633 or 785 nm depending of the nature of the sample. Measurements were taken with 10 s of exposure time and the laser spot was focused on the sample surface using a long working distance of 50× objective. The average Raman spectrum of each material was obtained with at least 10 measurements at different spots of the sample.

TEM micrographs were obtained using a Philips EM208 TEM and RADIUS 2.0 software (EMSIS GmbH, Muenster, Germany). The samples were dispersed in DCM and dropped onto a lacey carbon copper grid (300 mesh), the solvent was removed at room temperature overnight.

AFM was performed under ambient conditions using Multimode V7.30 (Veeco Instruments Inc., Santa Barbara, USA) with a NanoScope V controller (Digital Instruments, Santa Barbara, USA) working on tapping mode with a silicon tip (HQ:NSC15/Al BS probes from Mikromasch) at a working frequency of 235 kHz and a nominal force constant of 40 N m^{-1}. Height and phase images were simultaneously obtained. The samples were prepared by the immersion of a silicon wafer substrate in the organic phase and then it was dried with compressed air to avoid the restacking of the exfoliated material during the evaporation of the solvent (DCM).

UV-Vis-NIR measurements were carried out on a Cary 5000 Spectrometer (Varian), using 1 cm path quartz cuvettes.

For the preparation of expanded graphite, a GEX750 sonic tip (Sonics & Materials Inc.), 750 W power, stepped microtip, 3 mm tip diameter, and an amplitude of 160 μm, were used.

Conflicts of interest

There are no conflicts to declare.

Acknowledgements

M. P. is the AXA Chair for Bionanotechnology (2016–2023). This work was supported by the University of Trieste, INSTM, and the Italian Ministry of Education MIUR (cofin Prot. 2017PBXPN4). Part of this work was performed under the Maria de Maeztu Units of Excellence Program from the Spanish State Research Agency – grant no. MDM-2017-0720. M. B. acknowledges the ISCIII for the Sara Borrell research contract (CD18/00145).

Notes and references

1 K. S. Novoselov, A. K. Geim, S. V. Morozov, D. Jiang, Y. Zhang, S. V. Dubonos, I. V. Grigorieva and A. A. Firsov, *Science*, 2004, **306**, 666–669.
2 A. Wang, C. Wang, L. Fu, W. Wong-Ng and Y. Lan, *Nano-Micro Lett.*, 2017, **9**, 47.
3 D. V. Shtansky, K. L. Firestein and D. V. Golberg, *Nanoscale*, 2018, **10**, 17477–17493.
4 E. Singh, P. Singh, K. S. Kim, G. Y. Yeom and H. S. Nalwa, *ACS Appl. Mater. Interfaces*, 2019, **11**, 11061–11105.
5 V. Yadav, S. Roy, P. Singh, Z. Khan and A. Jaiswal, *Small*, 2019, **15**, 1803706.
6 Y. Kubota, K. Watanabe, O. Tsuda and T. Taniguchi, *Science*, 2007, **317**, 932–934.
7 K. Zhiqiao, C. Yulong, L. Yonglai, L. Li, H. Shui, W. Shipeng, M. Yingyan and Z. Liqun, *Small*, 2014, **11**, 1655–1659.
8 Z. Shi, X. Wang, Q. Li, P. Yang, G. Lu, R. Jiang, H. Wang, C. Zhang, C. Cong, Z. Liu, T. Wu, H. Wang, Q. Yu and X. Xie, *Nat. Commun.*, 2020, **11**, 849.
9 M. H. Khan, H. K. Liu, X. Sun, Y. Yamauchi, Y. Bando, D. Golberg and Z. Huang, *Mater. Today*, 2017, **20**, 611–628.
10 M. Gao, X. Jia, J. Ma, X. Fan, J. Gao and J. Xu, *Green Chem.*, 2021, **23**, 7115–7121.
11 W. Luo, Y. Wang, E. Hitz, Y. Lin, B. Yang and L. Hu, *Adv. Funct. Mater.*, 2017, **27**, 1701450.
12 K. F. Mak, C. Lee, J. Hone, J. Shan and T. F. Heinz, *Phys. Rev. Lett.*, 2010, **105**, 136805.
13 E. Yalon, C. J. McClellan, K. K. H. Smithe, M. Muñoz Rojo, R. L. Xu, S. V. Suryavanshi, A. J. Gabourie, C. M. Neumann, F. Xiong, A. B. Farimani and E. Pop, *Nano Lett.*, 2017, **17**, 3429–3433.
14 F. Yang, P. Song, M. Ruan and W. Xu, *FlatChem*, 2019, **18**, 100133.
15 S. Wang, J.-K. Huang, M. Li, A. Azam, X. Zu, L. Qiao, J. Yang and S. Li, *ACS Appl. Mater. Interfaces*, 2021, **13**, 47962–47971.

16 X. Liu, B. Li, F. A. Soto, X. Li, R. R. Unocic, P. B. Balbuena, A. R. Harutyunyan, J. Hone and D. V. Esposito, *ACS Catal.*, 2021, **11**, 12159–12169.
17 Q. Zhang, H. Ying, X. Li, R. Xiang, Y. Zheng, H. Wang, J. Su, M. Xu, X. Zheng, S. Maruyama and X. Zhang, *ACS Appl. Mater. Interfaces*, 2021, **13**, 31861–31869.
18 H. Wang, C. Li, P. Fang, Z. Zhang and J. Z. Zhang, *Chem. Soc. Rev.*, 2018, **47**, 6101–6127.
19 X. Zhang, X. Xie, H. Wang, J. Zhang, B. Pan and Y. Xie, *J. Am. Chem. Soc.*, 2013, **135**, 18–21.
20 K. C. Christoforidis, Z. Syrgiannis, V. La Parola, T. Montini, C. Petit, E. Stathatos, R. Godin, J. R. Durrant, M. Prato and P. Fornasiero, *Nano Energy*, 2018, **50**, 468–478.
21 L. Jiang, J. Li, K. Wang, G. Zhang, Y. Li and X. Wu, *Appl. Catal., B*, 2020, **260**, 118181.
22 P. Yang, H. Ou, Y. Fang and X. Wang, *Angew. Chem., Int. Ed.*, 2017, **56**, 3992–3996.
23 N. Tian, H. Huang, X. Du, F. Dong and Y. Zhang, *J. Mater. Chem. A*, 2019, **7**, 11584–11612.
24 M. Liras, M. Barawi and V. A. de la Peña O'Shea, *Chem. Soc. Rev.*, 2019, **48**, 5454–5487.
25 L. Yang, W. Chen, Q. Yu and B. Liu, *Nano Res.*, 2021, **14**, 1583–1597.
26 L. Niu, J. N. Coleman, H. Zhang, H. Shin, M. Chhowalla and Z. Zheng, *Small*, 2015, **12**, 272–293.
27 S. Witomska, T. Leydecker, A. Ciesielski and P. Samorì, *Adv. Funct. Mater.*, 2019, 1901126.
28 Z. Li, R. J. Young, C. Backes, W. Zhao, X. Zhang, A. A. Zhukov, E. Tillotson, A. P. Conlan, F. Ding, S. J. Haigh, K. S. Novoselov and J. N. Coleman, *ACS Nano*, 2020, **14**, 10976–10985.
29 K.-G. Zhou, N.-N. Mao, H.-X. Wang, Y. Peng and H.-L. Zhang, *Angew. Chem., Int. Ed.*, 2011, **50**, 10839–10842.
30 U. Halim, C. R. Zheng, Y. Chen, Z. Lin, S. Jiang, R. Cheng, Y. Huang and X. Duan, *Nat. Commun.*, 2013, **4**, 2213.
31 J. Shen, J. Wu, M. Wang, P. Dong, J. Xu, X. Li, X. Zhang, J. Yuan, X. Wang, M. Ye, R. Vajtai, J. Lou and P. M. Ajayan, *Small*, 2016, **12**, 2741–2749.
32 S. J. Woltornist, A. J. Oyer, J.-M. Y. Carrillo, A. V. Dobrynin and D. H. Adamson, *ACS Nano*, 2013, **7**, 7062–7066.
33 S. Biswas and L. T. Drzal, *Nano Lett.*, 2009, **9**, 167–172.
34 Z. Tang, J. Zhuang and X. Wang, *Langmuir*, 2010, **26**, 9045–9049.
35 S. J. Woltornist, D. Varghese, D. Massucci, Z. Cao, A. V. Dobrynin and D. H. Adamson, *Adv. Mater.*, 2017, **29**, 1604947.
36 F. Chen, D. Varghese, S. T. McDermott, I. George, L. Geng and D. H. Adamson, *Sci. Rep.*, 2020, **10**, 18047.
37 C.-X. Hu, Y. Shin, O. Read and C. Casiraghi, *Nanoscale*, 2021, **13**, 460–484.
38 A. Griffin, K. Nisi, J. Pepper, A. Harvey, B. M. Szydłowska, J. N. Coleman and C. Backes, *Chem. Mater.*, 2020, **32**, 2852–2862.
39 X. Wang and P. Wu, *ACS Appl. Mater. Interfaces*, 2018, **10**, 2504–2514.
40 R. Worsley, L. Pimpolari, D. McManus, N. Ge, R. Ionescu, J. A. Wittkopf, A. Alieva, G. Basso, M. Macucci, G. Iannaccone, K. S. Novoselov, H. Holder, G. Fiori and C. Casiraghi, *ACS Nano*, 2019, **13**, 54–60.
41 X. Wu, Y. Li, L. Chen, J. Zhao, B. Wu and Z.-B. Zhang, *Chem. Commun.*, 2020, **56**, 2035–2038.
42 Y. Xu, H. Cao, Y. Xue, B. Li, W. Cai, Y. Xu, H. Cao, Y. Xue, B. Li and W. Cai, *Nanomaterials*, 2018, **8**, 942.
43 A. Amiri, M. Naraghi, G. Ahmadi, M. Soleymaniha and M. Shanbedi, *FlatChem*, 2018, **8**, 40–71.
44 A. Ciesielski and P. Samorì, *Adv. Mater.*, 2016, **28**, 6030–6051.
45 H. Ye, X. Zhang, C. Xu, B. Han and L. Xu, *J. Mater. Chem. C*, 2018, **6**, 11144–11155.
46 W. Yin, X. Dong, J. Yu, J. Pan, Z. Yao, Z. Gu and Y. Zhao, *ACS Appl. Mater. Interfaces*, 2017, **9**, 21362–21370.
47 E. S. Da Silva, N. M. M. Moura, M. G. P. M. S. Neves, A. Coutinho, M. Prieto, C. G. Silva and J. L. Faria, *Appl. Catal., B*, 2018, **221**, 56–69.
48 A. A. Muhabie, C.-C. Cheng, J.-J. Huang, Z.-S. Liao, S.-Y. Huang, C.-W. Chiu and D.-J. Lee, *Chem. Mater.*, 2017, **29**, 8513–8520.
49 L. Gang and K. Naoki, *ChemPhysChem*, 2016, **17**, 1557–1567.
50 A. Schlierf, H. Yang, E. Gebremedhn, E. Treossi, L. Ortolani, L. Chen, A. Minoia, V. Morandi, P. Samorì, C. Casiraghi, D. Beljonne and V. Palermo, *Nanoscale*, 2013, **5**, 4205–4216.
51 H. Yang, F. Withers, E. Gebremedhn, E. Lewis, L. Britnell, A. Felten, V. Palermo, S. Haigh, D. Beljonne and C. Casiraghi, *2D Mater.*, 2014, **1**, 011012.
52 D. Parviz, S. Das, H. S. T. Ahmed, F. Irin, S. Bhattacharia and M. J. Green, *ACS Nano*, 2012, **6**, 8857–8867.
53 L. Zhang, Z. Zhang, C. He, L. Dai, J. Liu and L. Wang, *ACS Nano*, 2014, **8**, 6663–6670.
54 M. Chen, C. Yang, Z. Xu, Y. Tang, J. Jiang, P. Liu, Y. Su and D. Wu, *RSC Adv.*, 2016, **6**, 13666–13669.
55 D. H. Gharib, S. Gietman, F. Malherbe and S. E. Moulton, *Carbon*, 2017, **123**, 695–707.
56 D. H. Gharib, P. Lock, S. E. Moulton, F. Malherbe and S. J. Langford, *ChemNanoMat*, 2019, **5**, 1303–1310.
57 M. Marcia, A. Hirsch and F. Hauke, *FlatChem*, 2017, **1**, 89–103.
58 M. Marcia, C. Vinh, C. Dolle, G. Abellán, J. Schönamsgruber, T. Schunk, B. Butz, E. Spiecker, F. Hauke and A. Hirsch, *Adv. Mater. Interfaces*, 2016, **3**, 1600365.
59 J. M. Englert, J. Röhrl, C. D. Schmidt, R. Graupner, M. Hundhausen, F. Hauke and A. Hirsch, *Adv. Mater.*, 2009, **21**, 4265–4269.
60 N. V. Kozhemyakina, J. M. Englert, G. Yang, E. Spiecker, C. D. Schmidt, F. Hauke and A. Hirsch, *Adv. Mater.*, 2010, **22**, 5483–5487.
61 L. Martín-Gomis, N. Karousis, F. Fernández-Lázaro, I. D. Petsalakis, K. Ohkubo, S. Fukuzumi, N. Tagmatarchis

and Á. Sastre-Santos, *Photochem. Photobiol. Sci.*, 2017, **16**, 596–605.
62 S. R. Pathipati, E. Pavlica, A. Schlierf, M. El Gemayel, P. Samorì, V. Palermo and G. Bratina, *J. Phys. Chem. C*, 2014, **118**, 24819–24826.
63 F. Bausi, A. Schlierf, E. Treossi, M. G. Schwab, V. Palermo and F. Cacialli, *Org. Electron.*, 2015, **18**, 53–60.
64 A. Liscio, K. Kouroupis-Agalou, A. Kovtun, E. Gebremedhn, M. El Garah, W. Rekab, E. Orgiu, L. Giorgini, P. Samorì, D. Beljonne and V. Palermo, *ChemPlusChem*, 2017, **82**, 358–367.
65 F. Lu, F. Wang, W. Gao, X. Huang, X. Zhang and Y. Li, *Mater. Express*, 2013, **3**, 144–150.
66 X. Fu, J. Feng, X. Tan, Q. Lu, R. Yuan and S. Chen, *RSC Adv.*, 2015, **5**, 42698–42704.
67 G. Abellán, V. Lloret, U. Mundloch, M. Marcia, C. Neiss, A. Görling, M. Varela, F. Hauke and A. Hirsch, *Angew. Chem., Int. Ed.*, 2016, **55**, 14557–14562.
68 H. Beneš, R. K. Donato, P. Ecorchard, D. Popelková, E. Pavlová, D. Schelonka, O. Pop-Georgievski, H. S. Schrekker and V. Štengl, *RSC Adv.*, 2016, **6**, 6008–6015.
69 A. P. Godoy, P. Ecorchard, H. Beneš, J. Tolasz, D. Smržová, L. Seixas, J. J. Pedrotti, E. A. T. de Souza, O. A. El Seoud and R. K. Donato, *Ultrason. Sonochem.*, 2019, **55**, 279–288.
70 J. A. Berrocal, R. H. Zha, B. F. M. de Waal, J. A. M. Lugger, M. Lutz and E. W. Meijer, *ACS Nano*, 2017, **11**, 3733–3741.
71 S. Berardi, V. Cristino, M. Canton, R. Boaretto, R. Argazzi, E. Benazzi, L. Ganzer, R. Borrego Varillas, G. Cerullo, Z. Syrgiannis, F. Rigodanza, M. Prato, C. A. Bignozzi and S. Caramori, *J. Phys. Chem. C*, 2017, **121**, 17737–17745.
72 A. Ciesielski and P. Samorì, *Chem. Soc. Rev.*, 2014, **43**, 381–398.
73 B. Abismaïl, J. P. Canselier, A. M. Wilhelm, H. Delmas and C. Gourdon, *Ultrason. Sonochem.*, 1999, **6**, 75–83.
74 L. Liu, Y. P. Feng and Z. X. Shen, *Phys. Rev. B: Condens. Matter Mater. Phys.*, 2003, **68**, 104102.
75 X. Ling, W. Fang, Y.-H. Lee, P. T. Araujo, X. Zhang, J. F. Rodriguez-Nieva, Y. Lin, J. Zhang, J. Kong and M. S. Dresselhaus, *Nano Lett.*, 2014, **14**, 3033–3040.
76 Q. Pang and L. F. Nazar, *ACS Nano*, 2016, **10**, 4111–4118.
77 C. R. Martinez and B. L. Iverson, *Chem. Sci.*, 2012, **3**, 2191–2201.
78 A. Govind Rajan, V. Sresht, A. A. H. Pádua, M. S. Strano and D. Blankschtein, *ACS Nano*, 2016, **10**, 9145–9155.
79 M. Garrido, E. Martínez-Periñán, J. Calbo, L. Rodríguez-Pérez, J. Aragó, E. Lorenzo, E. Ortí, N. Martín and M. Á. Herranz, *J. Mater. Chem. C*, 2021, **9**, 10944–10951.
80 X. Li, G. Zhang, X. Bai, X. Sun, X. Wang, E. Wang and H. Dai, *Nat. Nanotechnol.*, 2008, **3**, 538.
81 W. Zhao, Y. Guo, S. Wang, H. He, C. Sun and S. Yang, *Appl. Catal., B*, 2015, **165**, 335–343.
82 Y.-H. Lee, X.-Q. Zhang, W. Zhang, M.-T. Chang, C.-T. Lin, K.-D. Chang, Y.-C. Yu, J. T.-W. Wang, C.-S. Chang, L.-J. Li and T.-W. Lin, *Adv. Mater.*, 2012, **24**, 2320–2325.
83 A. C. Ferrari, J. C. Meyer, V. Scardaci, C. Casiraghi, M. Lazzeri, F. Mauri, S. Piscanec, D. Jiang, K. S. Novoselov, S. Roth and A. K. Geim, *Phys. Rev. Lett.*, 2006, **97**, 187401.
84 K. R. Paton, E. Varrla, C. Backes, R. J. Smith, U. Khan, A. O'Neill, C. Boland, M. Lotya, O. M. Istrate, P. King, T. Higgins, S. Barwich, P. May, P. Puczkarski, I. Ahmed, M. Moebius, H. Pettersson, E. Long, J. Coelho, S. E. O'Brien, E. K. McGuire, B. M. Sanchez, G. S. Duesberg, N. McEvoy, T. J. Pennycook, C. Downing, A. Crossley, V. Nicolosi and J. N. Coleman, *Nat. Mater.*, 2014, **13**, 624–630.
85 S. Tonda, S. Kumar, S. Kandula and V. Shanker, *J. Mater. Chem. A*, 2014, **2**, 6772–6780.
86 Q. Cai, D. Scullion, A. Falin, K. Watanabe, T. Taniguchi, Y. Chen, E. J. G. Santos and L. H. Li, *Nanoscale*, 2017, **9**, 3059–3067.
87 L. H. Li, J. Cervenka, K. Watanabe, T. Taniguchi and Y. Chen, *ACS Nano*, 2014, **8**, 1457–1462.
88 Y. Ji, B. Calderon, Y. Han, P. Cueva, N. R. Jungwirth, H. A. Alsalman, J. Hwang, G. D. Fuchs, D. A. Muller and M. G. Spencer, *ACS Nano*, 2017, **11**, 12057–12066.
89 H. S. S. Ramakrishna Matte, A. Gomathi, A. K. Manna, D. J. Late, R. Datta, S. K. Pati and C. N. R. Rao, *Angew. Chem., Int. Ed.*, 2010, **49**, 4059–4062.
90 W. Liu, C. Zhao, R. Zhou, D. Zhou, Z. Liu and X. Lu, *Nanoscale*, 2015, **7**, 9919–9926.
91 D. Cortés-Arriagada, *Int. J. Quantum Chem.*, 2017, **117**, e25346.